

# Li + Li<sub>2</sub> Dissociation Reaction Using the Self-Consistent Potential and Trajectory Surface Hopping Methods

J. M. C. Marques, A. I. Voronin, and A. J. C. Varandas\*

Departamento de Química, Universidade de Coimbra, P-3049 Coimbra Codex, Portugal

Received: December 6, 2001; In Final Form: January 16, 2002

Self-consistent potential and trajectory surface hopping methods have been applied to study the Li + Li<sub>2</sub> dissociation reaction. Both methods fall into the classical trajectory methodology, with batches of 5000 trajectories being run over the translational energy range  $25 \leq E_{tr} \leq 100$  kcal mol<sup>-1</sup> keeping the internal state of Li<sub>2</sub> fixed at ( $v = 0, j = 10$ ). The effect of vibrational excitation has also been studied by running additional sets of trajectories for  $E_{tr} = 25$  kcal mol<sup>-1</sup> with ( $v = 10, j = 10$ ) and ( $v = 20, j = 10$ ). All dissociative cross sections have been calculated using realistic double many-body expansion potential energy surfaces. The importance of nonadiabatic effects is investigated.

## 1. Introduction

The theoretical treatment of chemical reactions usually involves the evaluation of the relevant electronic potential energy surfaces followed by the dynamics study of the nuclei motion. This procedure confines the standard Born–Oppenheimer approximation, which establishes the separability of the electronic and nuclear coordinates, with the corresponding electronic states being known as adiabatic. However, because of the nonadiabatic coupling among different electronic states, many chemical processes can be correctly described only if transition between two or more such states is allowed. In fact, the electronic states may closely approach each other or even intersect for certain geometries, and hence, finite values of the relative nuclear velocities may lead to nonadiabatic transitions among them. Nuclear dynamics studies using semiclassical methods must then allow for the trajectories to scan different electronically adiabatic states, which implies their hopping between the potential sheets under certain conditions. Such a goal has been accomplished in several trajectory surface hopping methods.<sup>1–6</sup>

An alternative approach to the problem consists of using a diabatic electronic basis, which allows in principle for the elimination of the nuclear momentum coupling associated to the adiabatic representation. For a two-state system, the diabatic potential matrix assumes the form

$$\mathbf{V} = \begin{pmatrix} V_{11} & V_{12} \\ V_{12} & V_{22} \end{pmatrix} \quad (1)$$

where the diagonal elements  $V_{ii}$  ( $i = 1, 2$ ) are the diabatic surfaces and  $V_{12}$  is the coupling term. Unlike the adiabatic states, the diabatic ones are not pure electronic states because they are coupled through  $V_{12}$ . However,  $V_{12}$  tends to zero at large internuclear distances, and hence, the diabatic surfaces will coincide with the adiabatic ones at such asymptotic regions. Note that the adiabatic potential energy surfaces (labeled  $V_+$  and  $V_-$ ) are the eigenvalues of the potential matrix in eq 1. Thus, once this is available, it is straightforward matter to obtain

$V_-$  and  $V_+$ . The result is

$$V_{\pm} = \frac{V_{11} + V_{22}}{2} \pm \left[ \left( \frac{V_{11} - V_{22}}{2} \right)^2 + V_{12}^2 \right]^{1/2} \quad (2)$$

However, it is impossible to unambiguously obtain all of the diabatic potential matrix elements from the corresponding adiabatic states,  $V_-$  and  $V_+$ , except if these are given by London–Eyring–Polanyi–Sato (LEPS)<sup>7–9</sup> functions. As applied to three interacting <sup>2</sup>S atoms, the semiempirical LEPS method consists of obtaining the Coulomb and exchange integrals from the two-body potentials for the ground-singlet and lowest-triplet states of the appropriate diatomic fragments. Although three-body energy contributions may be added to the matrix elements of eq 1, special care must be taken<sup>10</sup> to prevent the modified LEPS formalism from failing to reproduce the appropriate symmetry of the London equation.

The semiclassical self-consistent potential (SCP) method is best suited to use with a diabatic representation of the potential energy.<sup>11–18</sup> This methodology can be incorporated into the classical trajectory programs and consists of integrating simultaneously both the nuclear equations of motion and the time evolution of the electronic wave function. Moreover, the SCP method may employ an average over an ensemble of trajectories<sup>15–18</sup> (i.e., self-consistency in each individual trajectory depends on the other trajectories of the ensemble), although in most practical applications the potential energy dictating the nuclear motion is chosen to be consistent with the electronic density matrix elements calculated along each individual trajectory.<sup>11–14,18</sup>

In previous work,<sup>19</sup> we have used a trajectory surface hopping<sup>1</sup> (TSH) method to calculate the dissociative cross sections for the title reaction. Following motivations already outlined elsewhere,<sup>19–26</sup> our major goal in the present study is to report a detailed comparative analysis of the SCP and TSH methods by calculating the dissociation cross sections for the Li + Li<sub>2</sub> reaction using realistic potential matrices obtained from the double many-body expansion<sup>27</sup> (DMBE) method. Of course, a meaningful comparison of the SCP and TSH dissociative cross

sections is possible only when the potential is the same. For this purpose, we have conveniently modified the diabatic DMBE III potential energy surface<sup>28,29</sup> such that its diabaticization becomes straightforward (the new form so obtained will be denoted heretofore by DMBE III-D). To assess the modifications that were introduced, additional TSH calculations have been carried out using the DMBE III-D potential energy surface.

The plan of the paper is as follows. Section 2 describes the TSH and SCP methods, the DMBE III-D potential energy surface for Li<sub>3</sub>, and the corresponding diabatic potential matrix elements. The results are reported in section 3, where a detailed comparative discussion of both TSH and SCP dissociative cross sections for the Li + Li<sub>2</sub> reaction is also presented. The conclusions are in section 4.

## 2. Methods and Potential Energy Surface

**2.1. Trajectory Surface Hopping Method.** In the present study, we have used the TSH method of Tully and Preston.<sup>1</sup> Although the details concerning the TSH approach have been reported elsewhere,<sup>19</sup> we survey here a few remarks about it.

In the TSH method, the hop from one sheet to another is only allowed when the trajectory enters in the crossing seam, which has been detected as in previous work<sup>19</sup> by inspecting the difference,  $\Delta V = V_+ - V_-$ , between the two sheets of the potential energy surface along the trajectory path. Whenever  $\Delta V$  reaches a minimum value, the trajectory is halted and the values of  $V_-$  and  $V_+$  at the three last points are used to calculate the parameters of the Landau–Zener formula for the probability of nonadiabatic transition:

$$P_{LZ} = \exp(-2\pi A^2/(\hbar B u)) \quad (3)$$

In this equation,  $u$  is the velocity (which is associated with  $E_{tr}$ ), and  $A$  and  $B$  are parameters that define the splitting between the two sheets;<sup>19</sup>  $A$  is the smallest difference between  $V_-$  and  $V_+$  at the crossing seam. As usual, the comparison of  $P_{LZ}$  with a generated random number is used to decide whether the trajectory may hop to the other sheet. However, if the kinetic energy component used to correct for the potential gap is not large enough, the trajectory proceeds on the same surface and the hop is said to be classically forbidden.

The main reason for using the original version<sup>1</sup> of the TSH method is its simplicity in comparison with more sophisticated semiclassical approaches.<sup>2,4,6,30–35</sup> Among these, the Zhu–Nakamura theory (ref 35 and references therein) is probably the most suitable for solving the problem of classically forbidden hops.<sup>36</sup> However, the study of the Li + Li<sub>2</sub> dissociation uses a potential energy surface in which both lower and upper sheets cross, and then we do not expect the problem of classically forbidden hops to be serious in the present case; this is corroborated by the trajectory calculations of the present work. Moreover, the adequacy of the TSH method to describe nonadiabatic effects has been the subject of many investigations.<sup>37–39</sup> It has been shown to underestimate the relevant nonadiabatic transition probabilities when compared with exact quantum calculations.<sup>40,41</sup> In particular, Takayanagi et al.<sup>41</sup> have studied the nonadiabatic (D + H<sub>2</sub>)<sup>+</sup> reaction and concluded that the discrepancy between TSH and quantum results is due to the fact that nonadiabatic surface hopping takes place away from the crossing seam. Because both sheets cross at the locus defined by the conical intersection while separating from each other away from the seam, one expects the surface hopping to be quite localized for the title system.

**2.2. Self-Consistent Potential Method.** The dynamics approach used in the present work follows the spirit of the SCP method suggested by Meyer and Miller,<sup>11</sup> and more recently by Amarouche et al.<sup>18</sup> Unlike TSH,<sup>1–6</sup> which considers abrupt transitions among different adiabatic surfaces (leading as a result to drastic changes in the dynamics of the nuclei), the SCP method allows a “soft” evolution of the system under the action of an average mean field quantum potential, which is associated with the superposition of various electronic states.

According to the SCP method, the total Hamiltonian describing the motion of both electrons and nuclei assumes the form

$$\mathcal{H} = T_N + H_e \quad (4)$$

where  $T_N$  is the nuclear kinetic energy operator, and  $H_e$  is the electronic Hamiltonian for fixed nuclear positions. The evolution of the electronic wave function,  $\psi$ , is obtained rigorously by solving the time-dependent Schrödinger equation

$$i\hbar \frac{\partial |\psi(\mathbf{r}, t; \mathbf{R})\rangle}{\partial t} = H_e |\psi(\mathbf{r}, t; \mathbf{R})\rangle \quad (5)$$

In turn, the time-dependent electronic state vector,  $|\psi(\mathbf{r}, t; \mathbf{R})\rangle$  may be developed over the complete orthonormal time-independent  $|\phi_j\rangle$  basis as

$$|\psi(\mathbf{r}, t; \mathbf{R})\rangle = \sum_j a_j(t) |\phi_j(\mathbf{r}; \mathbf{R})\rangle \quad (6)$$

where  $\mathbf{r}$  and  $\mathbf{R}$  are the vectors of the electronic and nuclear coordinates, respectively, and the time dependence is given only through the complex amplitudes  $a_j$  (i.e.,  $a_j = \alpha_j + i\beta_j$ ). By replacing eq 6 into eq 5, multiplying from the left by  $\phi_k$  and integrating over  $\mathbf{r}$ , one obtains the following first-order differential equations for the  $a_j$  coefficients:

$$i\hbar \dot{a}_j = \sum_k a_k(t) H_{jk}(\mathbf{R}) - i\hbar \sum_k a_k(t) \dot{\mathbf{R}} \cdot \mathbf{d}_{jk}(\mathbf{R}) \quad (7)$$

where  $\dot{a}_j$  and  $\dot{\mathbf{R}}$  are the time derivatives of both amplitudes ( $a_j$ ) and coordinates ( $\mathbf{R}$ ), and

$$H_{jk}(\mathbf{R}) = \langle \phi_j(\mathbf{r}; \mathbf{R}) | H_e(\mathbf{r}; \mathbf{R}) | \phi_k(\mathbf{r}; \mathbf{R}) \rangle \quad (8)$$

$$\mathbf{d}_{jk}(\mathbf{R}) = \langle \phi_j(\mathbf{r}; \mathbf{R}) | \nabla_{\mathbf{R}} \phi_k(\mathbf{r}; \mathbf{R}) \rangle \quad (9)$$

are the electronic Hamiltonian matrix elements and the nonadiabatic coupling vectors, respectively. Note that, for a diabatic basis, eq 7 reduces to the first term because the vectors  $\mathbf{d}_{jk}$  vanish, while eq 8 may be identified with the matrix of eq 1 when only two electronic states are considered. Conversely, for adiabatic bases, the nonadiabatic coupling vectors are nonzero, while the off-diagonal elements of the potential matrix disappear (the diagonal elements are the adiabatic potential energy surfaces).

When a diabatic basis is used, the Hamiltonian of eq 4 in the SCP method assumes the form

$$\mathcal{H} = \sum_i \frac{p_N^2}{2m_N} + \sum_{j,k} |\phi_j\rangle H_{jk}(\mathbf{R}) \langle \phi_k| \quad (10)$$

where  $m_N$  is the mass associated with the nuclear coordinate,  $q_N(\mathbf{R})$ , of which the term  $p_N$  is the conjugate momentum, and  $H_{jk}$  are the diabatic electronic Hamiltonian matrix elements as

given in eq 8. Thus, the Hamilton equations of motion assume the form<sup>18</sup>

$$\dot{q}_N = \frac{\partial \mathcal{K}}{\partial p_N} = \frac{p_N}{m_N} \quad (11)$$

$$\dot{p}_N = - \left\langle \psi(\mathbf{r}, t; \mathbf{R}) \left| \frac{\partial H_e}{\partial q_N} \right| \psi(\mathbf{r}, t; \mathbf{R}) \right\rangle = \sum_{j,k} (\alpha_j \alpha_k + \beta_j \beta_k) \frac{\partial V_{jk}}{\partial q_N} \quad (12)$$

while the time evolution of the wave function  $\psi$  is accomplished in a self-consistent manner through the integration of the real ( $\alpha_j$ ) and imaginary ( $\beta_j$ ) parts of the amplitudes  $a_j$ , that is, by solving the equations

$$\dot{\alpha}_j = \sum_k \beta_k H_{jk} \quad (13)$$

$$\dot{\beta}_j = - \sum_k \alpha_k H_{jk} \quad (14)$$

where  $j$  labels the diabatic electronic state. Because only two electronic states of the title system have been considered, the differential equations 13 and 14 reduce to

$$\dot{\alpha}_j = \beta_1 V_{1j} + \beta_2 V_{j2} \quad (15)$$

$$\dot{\beta}_j = -\alpha_1 V_{1j} - \alpha_2 V_{j2} \quad (j = 1, 2) \quad (16)$$

where the elements  $H_{jk}$  ( $j, k = 1-2$ ) have been denoted  $V_{11}$ ,  $V_{22}$ , and  $V_{12}$  in the two-state potential matrix of eq 1. Moreover, the mean-field potential energy of the system may be written as

$$V_{\text{mean}} = (\alpha_1^2 + \beta_1^2)V_{11} + (\alpha_2^2 + \beta_2^2)V_{22} + 2(\alpha_1\alpha_2 + \beta_1\beta_2)V_{12} \quad (17)$$

Of course, the contribution (probability) of each diabatic state to the mean field at time  $t$  is given by the modulus of  $a_j(t)$ :

$$P_r^j(t) = a_j(t)a_j^*(t) = \alpha_j(t)^2 + \beta_j(t)^2 \quad (18)$$

where  $a_j^* = \alpha_j - i\beta_j$ . Because the probability of being in a given state changes with time, the trajectory may end in a nonpure state, which is a drawback of the SCP method. However, this is of little importance for the dissociation study of the present work because both  $V_{11}$  and  $V_{22}$  approach the same Li(<sup>2</sup>S) + Li(<sup>2</sup>S) + Li(<sup>2</sup>S) dissociation limit.

The time evolution of the title system is then achieved by simultaneous integration of the differential equations in eqs 11, 12, 15, and 16. In turn, the initial conditions for eqs 15 and 16 have been established as

$$\alpha_1 = \alpha_2 = \beta_2 = 0 \quad (19)$$

$$\beta_1 = 1 \quad (20)$$

which means that only the  $V_{11}$  diabatic state contributes initially to  $V_{\text{mean}}$ , in agreement with the fact that the Li<sub>2</sub> reactant molecule is expected to be in the ground singlet electronic state (see also subsection 2.3). As usual, the initial conditions for the Hamilton equations [eqs 11 and 12] are defined as for the TSH calculations.<sup>19</sup>

**2.3. Adiabatic and Diabatic Potential Energy Surfaces.** The study of the reaction  $\text{Li} + \text{Li}_2(X^1\Sigma_g^+) \rightarrow \text{Li} + \text{Li} + \text{Li}$  involves the knowledge of the potential energy surface for Li<sub>3</sub>. In a

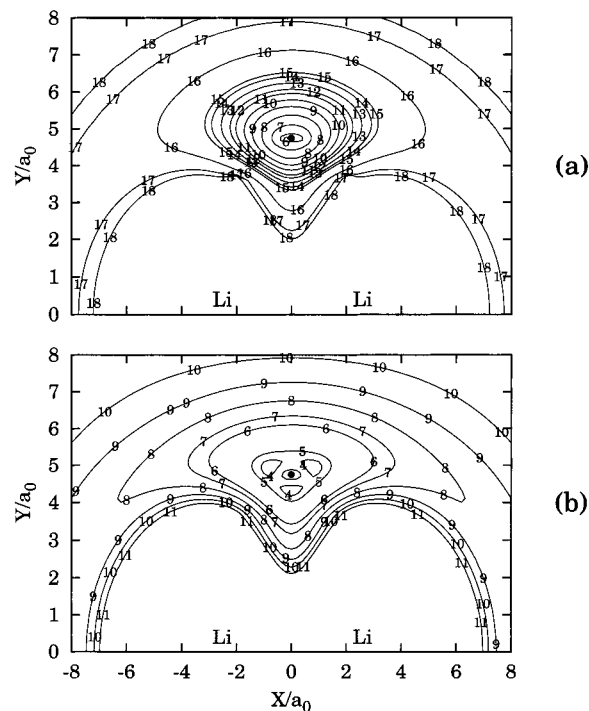


**Figure 1.** DMBE III contour plot for Li moving around a partially relaxed Li<sub>2</sub> ( $4.5a_0 \leq R_{\text{Li-Li}} \leq 8.0a_0$ ), which lies along the  $x$ -axis with the center of mass fixed at the origin: (a) upper sheet; (b) lower sheet. Contours 6–18 in panel a correspond to  $-0.05495$ ,  $-0.0527$ ,  $-0.0494$ ,  $-0.0460$ ,  $-0.0430$ ,  $-0.0400$ ,  $-0.0380$ ,  $-0.0350$ ,  $-0.0320$ ,  $-0.0300$ ,  $-0.0200$ ,  $-0.0100$ , and  $-0.005 E_h$ , respectively, while in panel b the contours  $-0.0595$ ,  $-0.0590$ ,  $-0.0547$ ,  $-0.0527$ ,  $-0.0494$ ,  $-0.0460$ ,  $-0.0430$ , and  $-0.0400 E_h$  are labelled 4–11, respectively. The conical intersection is indicated by the solid dots.

previous TSH study of the title reaction,<sup>19</sup> we have used the realistic two-valued DMBE III potential energy surface,<sup>28,29</sup> which correctly accounts for the conical intersection between the  $V_-$  and  $V_+$  adiabatic states. It has the form<sup>28,29</sup>

$$V_{\pm} = X'_{\text{LEPS}} + X_{\text{EHF}}^{(3)} \pm \frac{1}{2} [Y'_{\text{LEPS}} + Y_{\text{EHF}}^{(3)}]^{1/2} + \sum_{i=1}^3 V_{\text{DC},i}^{(2)} + V_{\text{DC}}^{(3)} \quad (21)$$

where  $X$  and  $Y$  are the Coulomb and exchange integrals of the LEPS formalism. Note the energy partition into extended-Hartree-Fock (EHF) and dynamical correlation (DC) terms, as is usually done in DMBE theory.<sup>42,43</sup> Note further that the prime in  $X'_{\text{LEPS}}$  and  $Y'_{\text{LEPS}}$  implies that these terms are obtained from the EHF curves alone. Note especially that eq 21 includes both two-body and three-body energy contributions; see also ref 28. In particular,  $Y_{\text{EHF}}^{(3)}$  is written as

$$Y_{\text{EHF}}^{(3)} = Y'_{\text{LEPS}} k \exp[-\tilde{d}(1/\sqrt{3} \sum_{i=1}^3 \rho_i)^2] \quad (22)$$

where  $\rho_i = R_i - R_i^0$  are displacement coordinates relative to a reference  $D_{3h}$  structure and  $k = -0.4135$  and  $\tilde{d} = 0.1a_0^{-2}$  are parameters.

To achieve a prompt diabaticization of the DMBE III potential energy surface, we have assumed that the exchange energy in eq 22 can be approximated by  $Y_{\text{EHF}}^{(3)} = Y'_{\text{LEPS}}$ , leading to DMBE III-D. Although such an approximation is not expected to give substantially different adiabatic potential energy surfaces, one observes from the contour plots of Figures 1 and 2 that the lower

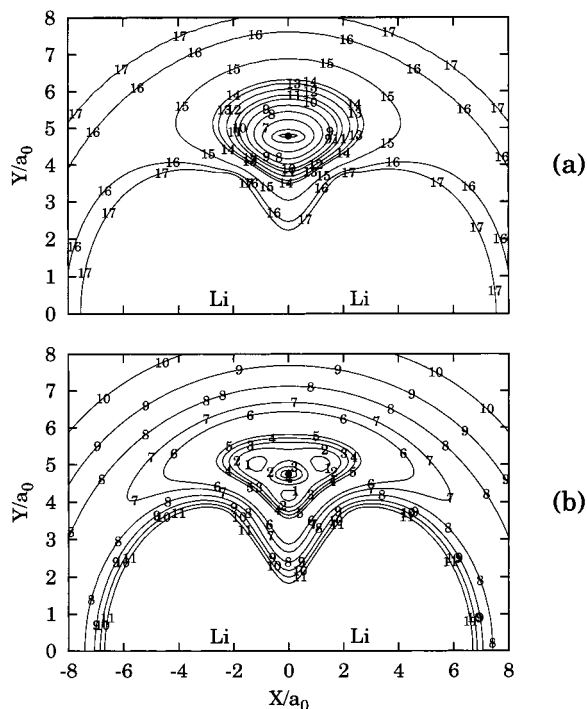


**Figure 2.** DMBE III-D contour plot for Li moving around a partially relaxed  $\text{Li}_2$  ( $4.5a_0 \leq R_{\text{Li-Li}} \leq 8.0a_0$ ), which lies along the  $x$ -axis with the center of mass fixed at the origin: (a) upper sheet; (b) lower sheet. Contours 5–17 in panel a correspond to  $-0.0540$ ,  $-0.0527$ ,  $-0.0494$ ,  $-0.0460$ ,  $-0.0430$ ,  $-0.0400$ ,  $-0.0380$ ,  $-0.0350$ ,  $-0.0320$ ,  $-0.0300$ ,  $-0.0200$ ,  $-0.0100$ , and  $-0.005 E_h$ , respectively, while in panel b the energies  $-0.0610$ ,  $-0.0605$ ,  $-0.0600$ ,  $-0.0595$ ,  $-0.0590$ ,  $-0.0547$ ,  $-0.0527$ ,  $-0.0494$ ,  $-0.0460$ ,  $-0.0430$ , and  $-0.0400 E_h$  are labeled 1–11, respectively. The conical intersection is indicated by the solid dots.

sheet of the  $\text{Li}_3$  DMBE III-D surface is more attractive than DMBE III, while the reverse is true for the upper sheet.

Using the DMBE III-D potential energy surface, we then obtain the diabatic potential matrix elements as described elsewhere by one of us.<sup>10</sup> Thus, the diagonal elements of eq 1 assume the form

$$V_{11} = \sum_{i=1}^3 V_i^{(2)}({}^1\Sigma_g^+, R_i) - \frac{3}{2}(J_1 + J_3) + X_{\text{EHF}}^{(3)} + V_{\text{DC}}^{(3)} \quad (23)$$

$$V_{22} = \sum_{i=1}^3 V_i^{(2)}({}^3\Sigma_u^+, R_i) + \frac{3}{2}(J_1 + J_3) + X_{\text{EHF}}^{(3)} + V_{\text{DC}}^{(3)} \quad (24)$$

where the exchange integrals  $J_i \equiv J(R_i)$  ( $i = 1-3$ ) are given only by the EHF singlet and triplet energy curves.<sup>28</sup> Figure 3a shows a contour plot of  $V_{11}$  for the Li atom moving around the  $\text{Li}_2$  reactant molecule, while a similar plot is presented in Figure 3b for  $V_{22}$ . The most interesting feature in both plots is the minimum ( $V_{11} = -0.0606E_h$  and  $V_{22} = -0.0612E_h$ ) appearing at  $R_1 = R_3 = 5.83a_0$  and  $R_2 = 5.01a_0$  in Figure 3a, and  $R_1 = R_3 = 5.22a_0$  and  $R_2 = 6.29a_0$  in Figure 3b. Additionally, the off-diagonal element  $V_{12}$  is written as

$$V_{12} = \frac{\sqrt{3}}{2}(J_1 - J_3) \quad (25)$$

Note that the electronic coupling  $V_{12}$  depends only on  $R_1$  and  $R_3$  and hence vanishes when these internuclear distances go to infinity. Because in the present dynamics calculations the reactant  $\text{Li}_2$  molecule is associated with the  $R_2$  internuclear

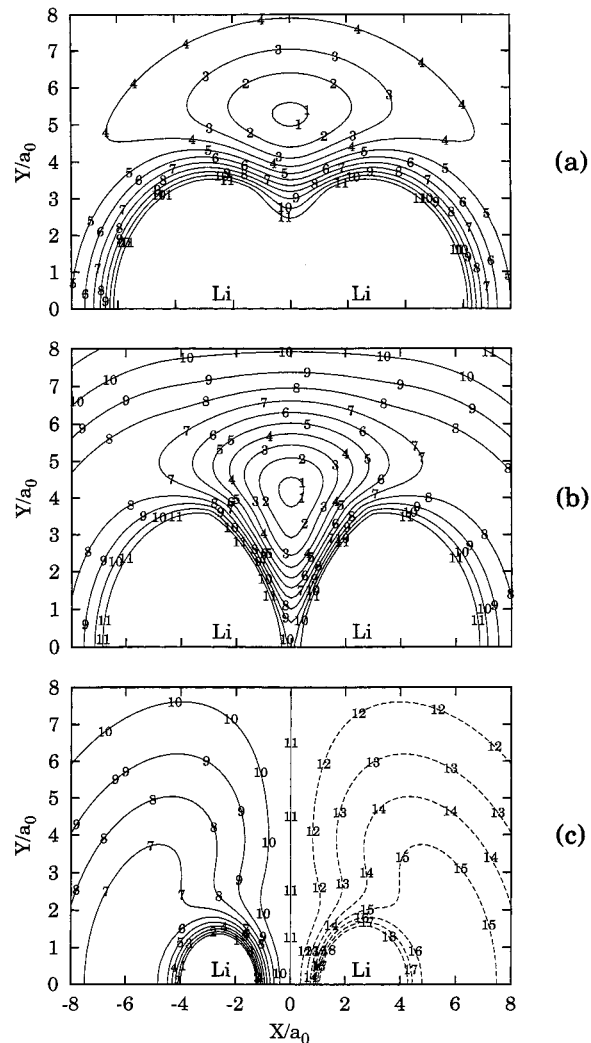


**Figure 3.** Contour plot of the diabatic matrix elements for Li moving around  $\text{Li}_2$ , which lies along the  $x$ -axis with the center of mass fixed at the origin: (a)  $V_{11}$ ; (b)  $V_{22}$ ; (c)  $V_{12}$ . The contours start at  $-0.06 E_h$  ( $-0.05 E_h$ ) in panels a and b (panel c) and are equally spaced by  $0.005 E_h$  in the three panels. In panels a and b, the  $\text{Li}_2$  molecule has been partially relaxed ( $4.5a_0 \leq R_2 \leq 8.0a_0$ ), while for the  $R_2$ -independent  $V_{12}$  diabatic matrix element (panel c) the Li–Li internuclear distance is fixed at its equilibrium geometry (i.e.,  $R_2 = 5.05a_0$ ). In panel c, the zero of energy corresponds to contour 11, the positive contours being shown in dashed lines.

distance, the  $V_{12}$  term is very small at the beginning of the trajectory. This is shown by the contour plot of Figure 3c, where it is clear that  $V_{12}$  is important only for small  $R_1$  or  $R_3$  distances. In contrast, for the perpendicular approach of the Li atom to the center of mass of  $\text{Li}_2$  (i.e., the vertical line at  $X = 0a_0$  in Figure 3c), the electronic coupling vanishes; in fact, eq 25 shows that  $V_{12} = 0E_h$  whenever  $R_1 = R_3$ . Another interesting feature of  $V_{12}$  is the symmetry displayed in Figure 3c: the right-hand side of the plot corresponds to positive energies, while the left part is associated with negative ones.

### 3. Results and Discussion

**3.1. Trajectory Calculations.** Batches of 5000 trajectories have been carried out for  $\text{Li} + \text{Li}_2$  ( $v = 0, j = 10$ ) collisions over the range of translational energies  $25 \leq E_{\text{tr}} \leq 100 \text{ kcal mol}^{-1}$  using the DMBE III-D potential energy surface and both the TSH and SCP methods described in section 2. Figure 4 shows that this range of translational energies is enough to obtain



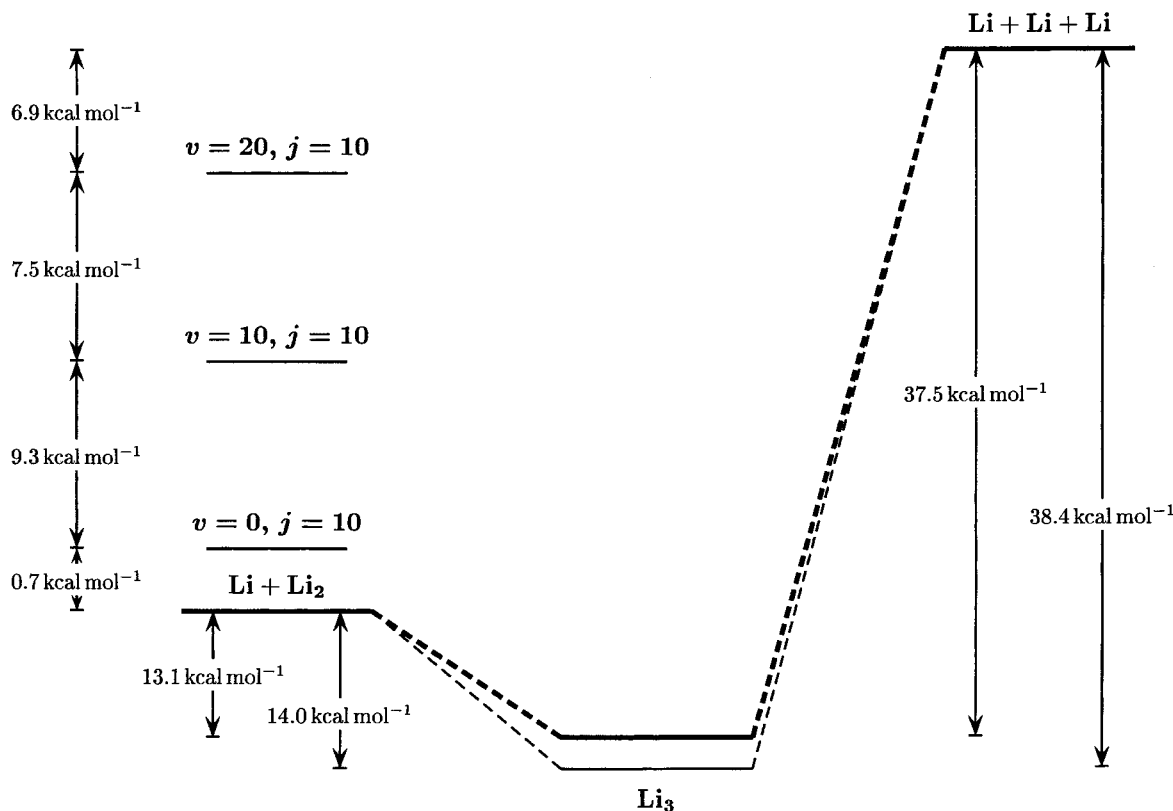


**Figure 4.** Schematic representation of the energetic features for the title reaction using both the DMBE III (thick lines) and DMBE III-D (thin lines) potential energy surfaces.

**TABLE 1: Comparison of the TSH Li + Li<sub>2</sub> Dissociation Results Using Both the DMBE III<sup>a</sup> (first entry) and DMBE III-D Potential Energy Surfaces (second entry)**

$E_{tr}$ , kcal mol <sup>-1</sup>	$\nu$	$b_{max}$ , $a_0$	adiabatic		nonadiabatic		$\sigma_d$ , $a_0^2$
			$N$	$\sigma$ , $a_0^2$	$N$	$\sigma$ , $a_0^2$	
25.0	0	5.7	59	1.2 ± 0.2	108	2.2 ± 0.2	3.4 ± 0.3
		5.7	67	1.4 ± 0.2	124	2.5 ± 0.2	3.9 ± 0.3
10	12.5	6.25	632	62.0 ± 2.3	115	11.3 ± 1.0	73.3 ± 2.5
		6.25	581	57.0 ± 2.2	100	9.8 ± 1.0	66.8 ± 2.4
20	14.0	13.20	1620	162.6 ± 3.8	125	15.4 ± 1.4	178.0 ± 4.0
		14.0	1433	176.5 ± 3.9	107	13.2 ± 1.3	189.6 ± 4.0
30.0	0	6.5	241	6.4 ± 0.4	369	9.8 ± 0.5	16.2 ± 0.6
		6.5	227	6.0 ± 0.4	286	7.6 ± 0.4	13.6 ± 0.6
40.0	0	6.25	582	14.3 ± 0.6	402	9.9 ± 0.5	24.2 ± 0.7
		6.25	581	14.3 ± 0.6	369	9.1 ± 0.5	23.3 ± 0.7
50.0	0	6.1	830	19.4 ± 0.6	421	9.8 ± 0.5	29.2 ± 0.7
		6.1	873	20.4 ± 0.6	404	9.4 ± 0.5	29.9 ± 0.7
80.0	0	5.8	1220	25.8 ± 0.6	511	10.8 ± 0.4	36.6 ± 0.7
		5.8	1332	28.2 ± 0.7	392	8.3 ± 0.4	36.4 ± 0.7
100.0	0	5.8	1317	27.8 ± 0.6	585	12.4 ± 0.5	40.2 ± 0.7
		5.8	1365	28.8 ± 0.7	457	9.7 ± 0.4	38.5 ± 0.7

<sup>a</sup> The values for  $E_{tr} = 25, 30, 40, 50,$  and  $80$  kcal mol<sup>-1</sup> have been taken from previous work.<sup>19</sup>

dissociation of Li<sub>2</sub>. For  $E_{tr} = 25$  kcal mol<sup>-1</sup>, we have run additional batches of 5000 trajectories for diatomic vibrational quantum numbers  $\nu = 10$  and 20. To get further insight on the dissociation dynamics at both low and high energies, two types of Li–Li<sub>2</sub> collisions have been considered: parallel (a) and perpendicular (b) attacks to the Li<sub>2</sub> axis. For both cases a and b, we have run batches of 5000 trajectories using the SCP and TSH methods at  $E_{tr} = 25$  kcal mol<sup>-1</sup> ( $\nu = 0, 10,$  and 20) and  $E_{tr} = 80$  kcal mol<sup>-1</sup> ( $\nu = 0$ ). In all cases, the initial Li<sub>2</sub> rotational quantum number has been fixed at  $j = 10$ . The TSH trajectory results are in Table 1, while the SCP ones are in Table 2; a comparison between the SCP and TSH dissociative cross

**TABLE 2: Trajectory Results Using the SCP Method**

$E_{tr}$ , kcal mol <sup>-1</sup>	$\nu$	$b_{max}$ , $a_0$	$N$	$\sigma_d$ , $a_0^2$
25.0	0	7.2	112	3.6 ± 0.3
	10	12.5	721	70.8 ± 2.4
	20	14.0	1515	186.6 ± 4.0
30.0	0	7.2	495	16.1 ± 0.7
	0	7.0	841	25.9 ± 0.8
50.0	0	6.8	1138	33.1 ± 0.9
	0	6.6	1299	35.6 ± 0.8
80.0	0	6.3	1613	40.2 ± 0.8
	0	6.3	1716	42.8 ± 0.8

**TABLE 3: Comparison of SCP and TSH Total Dissociative Cross Sections for Parallel (||) and Perpendicular (⊥) Li–Li<sub>2</sub> Attacks<sup>a</sup>**

$E_{tr}$ , kcal mol <sup>-1</sup>	$\nu$	SCP method		TSH method	
		$\sigma_{  }$ , $a_0^2$	$\sigma_{\perp}$ , $a_0^2$	$\sigma_{  }$ , $a_0^2$	$\sigma_{\perp}$ , $a_0^2$
25.0	0	3.8 ± 0.4	2.9 ± 0.3	4.6 ± 0.3	2.8 ± 0.2
	10	64.7 ± 2.3	82.8 ± 2.6	60.6 ± 2.3	81.5 ± 2.6
	20	161.4 ± 3.8	250.5 ± 4.3	168.0 ± 3.9	239.6 ± 4.2
80.0	0	36.6 ± 0.8	48.6 ± 0.9	30.2 ± 0.7	45.1 ± 0.7

<sup>a</sup> The values of  $b_{max}$  are the same as those presented in Tables 1 and 2.

sections for both parallel and perpendicular Li–Li<sub>2</sub> collisions is in Table 3. Also given for comparison in the first entries of Table 1 are the TSH results from previous work<sup>19</sup> using the DMBE III potential energy surface.<sup>28,29</sup> For completeness, similar TSH calculations have been carried out here for  $E_{tr} = 100$  kcal mol<sup>-1</sup>.

**3.2. TSH Dissociative Cross Sections.** Table 1 shows that the (adiabatic) dissociations taking place on the lower sheets of the DMBE III and DMBE III-D potential energy surfaces are in good agreement with each other for calculations up to  $E_{tr} = 50$  kcal mol<sup>-1</sup>. At higher translational energies, the results

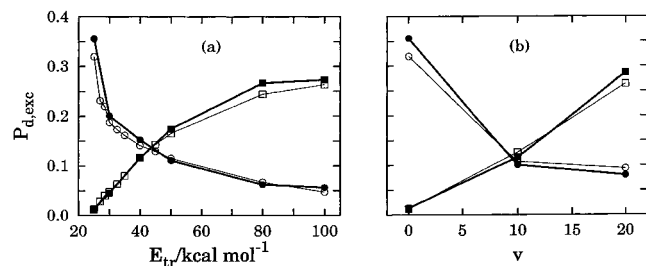


**Figure 5.** Probability of adiabatic dissociation (squares) and exchange (circles) for both DMBE III (thin line) and DMBE III-D (thick line) potential energy surfaces as a function of (a) translational energy and (b) initial vibrational quantum number.

using DMBE III-D become larger than those using DMBE III. Of course, at lower energies, the competition between the reactive (exchange) and dissociative processes favors the former. Because the lower sheet is more attractive in DMBE III-D for the approaching reactants (see Figure 4), this may explain why the adiabatic exchange probabilities are larger in this case; see Figure 5a. As expected, for increasing translational energies, the adiabatic dissociation becomes dominant, especially at  $E_{tr} \geq 50 \text{ kcal mol}^{-1}$  (Figure 5a). Note that, for  $E_{tr} = 80 \text{ kcal mol}^{-1}$ , the dissociative cross sections are larger for DMBE III-D, while at  $E_{tr} = 100 \text{ kcal mol}^{-1}$ , they become similar, which may be due to the fact that the differences in the potential wells then become irrelevant.

The nonadiabatic dissociation is expected to depend mainly on (i) the topography of the lower and upper sheets in DMBE III and DMBE III-D and (ii) the number of times that the trajectory crosses the seam. The first has implications on the transition probability between the lower ( $V_-$ ) and upper ( $V_+$ ) sheets, which in TSH is given by eq 3. Because the upper (lower) sheet of DMBE III-D potential energy surface (Figure 2) is more repulsive (attractive) than the corresponding DMBE III one (Figure 1),  $A$  in eq 3 is expected to be larger for DMBE III-D. Thus, the Landau–Zener transition probability is smaller for DMBE III-D than for DMBE III, in agreement with the calculated nonadiabatic cross sections. Moreover, the number of times that the trajectory enters the crossing seam has been shown<sup>25</sup> to be directly related to the trajectory lifetime ( $\tau$ ), of which the mean value ( $\tau_m$ ) decreases<sup>25</sup> with  $E_{tr}$  for DMBE III; a similar result is obtained for DMBE III-D. For example, the  $\tau_m$  values obtained with DMBE III (DMBE III-D) are (in au)  $0.73 \times 10^5$  ( $0.74 \times 10^5$ ),  $0.34 \times 10^5$  ( $0.34 \times 10^5$ ), and  $0.12 \times 10^5$  ( $0.12 \times 10^5$ ) for  $E_{tr} = 25, 30,$  and  $100 \text{ kcal mol}^{-1}$ , respectively. Accordingly, the average number of times that a dissociative trajectory crosses the seam is 8.0 (7.9), 4.1 (4.1), and 2.5 (2.5) for  $E_{tr} = 25, 30,$  and  $100 \text{ kcal mol}^{-1}$  using DMBE III (DMBE III-D). Thus, issue ii cannot explain the differences in the above results.

The total dissociative cross sections (adiabatic plus nonadiabatic) are in column eight of Table 1 and arise as a balance of the above observations. This explains the good agreement between the values of  $\sigma_d$  in DMBE III and DMBE III-D for all translational energies, except  $E_{tr} = 30$  and  $100 \text{ kcal mol}^{-1}$ . The higher values for DMBE III are due to the fact that the adiabatic dissociation is similar for both potential energy surfaces while nonadiabatic dissociation dominates for DMBE III.

Table 1 shows also the dissociative cross sections as a function of the vibrational quantum number of  $\text{Li}_2$  for  $E_{tr} = 25 \text{ kcal mol}^{-1}$ . Clearly, for  $v = 0$  and  $v = 10$ , the agreement between the results from DMBE III and DMBE III-D is good. However, as  $v$  increases to 20, the dissociative cross section becomes larger for DMBE III-D, while similar values are

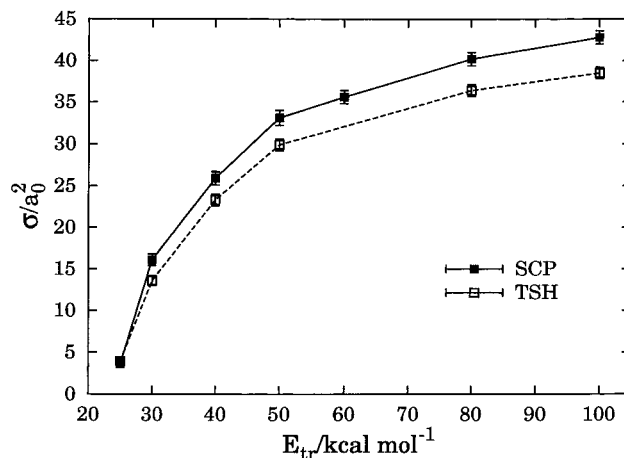


**Figure 6.** Dissociative cross sections for the  $\text{Li}_3$  DMBE III-D potential energy surface. The open squares are the TSH results, while the full squares represent the SCP ones.

obtained on both surfaces for nonadiabatic dissociation. In fact, Figure 5b shows that adiabatic exchange dominates over adiabatic dissociation for  $v = 0$ . One therefore expects that particular features of the two potential energy surfaces (e.g., the long-range attractive part) are more relevant to explain the larger value of the exchange probability ( $P_{exc}$ ) for DMBE III-D. As  $v$  increases, the  $\text{Li}_2$  reactant diatomic gets further stretched making dissociation dominate; the differences in the lower sheets of the two potentials are then likely to influence the dissociative cross sections. In fact, Figure 5b shows that the dissociation probability for  $v = 20$  increases significantly for the more attractive DMBE III-D.

**3.3. Comparison between TSH and SCP Results.** A major goal of the present work is to make a comparison between the traditional TSH method and the mean field SCP approach discussed in section 2.2. Because the Hamiltonian matrix applied in SCP uses the DMBE III-D potential energy surface, we must compare these results with the TSH ones reported in the second entries of Table 1. Table 2 shows the total SCP dissociative cross sections, while Figure 6 compares them with the TSH ones. As Figure 6 shows, the dissociative cross sections obtained by both methods are coincident within the error bars for  $E_{tr} = 25 \text{ kcal mol}^{-1}$  ( $v = 0$ ), while for higher translational energies the SCP results become largest. This general trend may be rationalized through inspection of Figures 2b and 3a, which illustrate the adiabatic  $V_-$  and diabatic  $V_{11}$  states acting in the initial stages of the TSH and SCP trajectories. As observed from these figures, the minimum of the  $V_{11}$  potential appears for larger  $\text{Li}-\text{Li}_2$  distances than in  $V_-$  for DMBE III-D. One then expects large impact parameter trajectories to be more efficiently captured by the attractive part of  $V_{11}$  than  $V_-$ , which explains the increase on the SCP dissociative cross section. This is corroborated from Tables 1 and 2, which show that the maximum impact parameter ( $b_{max}$ ) is in general larger for SCP than for TSH.

Figure 7 shows the  $v = 0$  opacity functions for  $E_{tr} = 25, 30, 80,$  and  $100 \text{ kcal mol}^{-1}$ . It is seen that they have similar shapes for both SCP and TSH. However, as mentioned above, larger values of the impact parameter tend to favor dissociation more for SCP than TSH. Another interesting feature refers to the opacity functions that show a maximum at intermediate impact parameters, especially for low energies. In fact, dissociation is not the major event at low-energy regimes, leading one to expect that small values of  $b$  contribute preferentially to nonreactive and exchange trajectories.

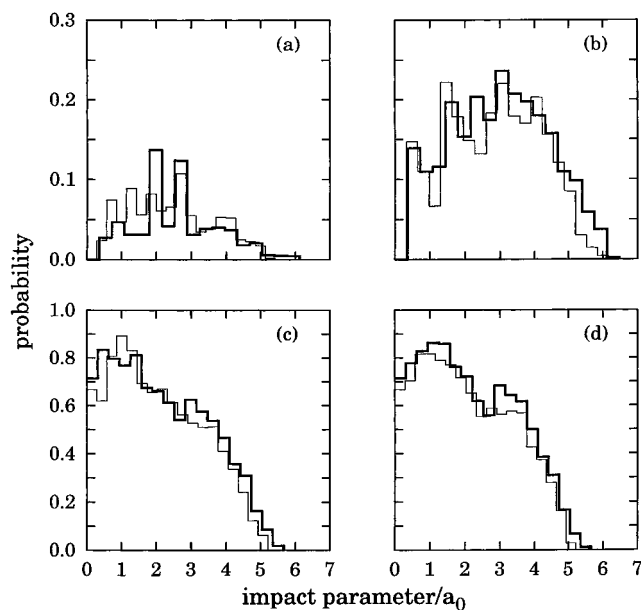


**Figure 7.** Opacity function for SCP (thick line) and TSH (thin line) methods: (a)  $E_{tr} = 25 \text{ kcal mol}^{-1}$ ; (b)  $E_{tr} = 30 \text{ kcal mol}^{-1}$ ; (c)  $E_{tr} = 80 \text{ kcal mol}^{-1}$ ; (d)  $E_{tr} = 100 \text{ kcal mol}^{-1}$ . In all cases,  $\nu = 0$ .

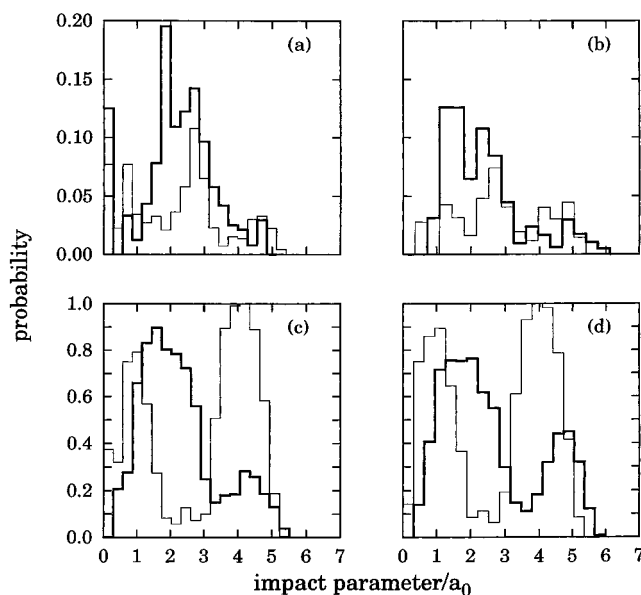


**Figure 8.** Opacity function for parallel (thick line) and perpendicular (thin line) Li–Li<sub>2</sub> attacks at  $E_{tr} = 25 \text{ kcal mol}^{-1}$  (panels a and b) and  $E_{tr} = 80 \text{ kcal mol}^{-1}$  (panels c and d) using both TSH (panels a and c) and SCP (panels b and d) methods. In all cases,  $\nu = 0$ .

Because the opacity functions of Figure 7 result from averaging over all Li–Li<sub>2</sub> approaching angles, it is difficult to analyze the importance of specific features of the potential energy surface. Thus, a study of parallel and perpendicular approaches of the Li atom to Li<sub>2</sub> may be illuminating to understand the influence of attractive and repulsive tails of the interaction potential on the dissociative process. Figure 8 shows the corresponding opacity functions at  $E_{tr} = 25$  and  $80 \text{ kcal mol}^{-1}$  for both SCP and TSH methods. As shown in Figure 8a,b for  $E_{tr} = 25 \text{ kcal mol}^{-1}$  ( $\nu = 0$ ), the parallel approach leads to larger reaction probabilities, peaking the opacity function at  $b \approx 2a_0$ . This suggests that head-on collisions may play an important role on dissociation; see also Figures 2b and 3a. Conversely, the opacity functions for  $E_{tr} = 80 \text{ kcal mol}^{-1}$  ( $\nu = 0$ ) (Figure 8c,d) show a bimodal structure for both parallel

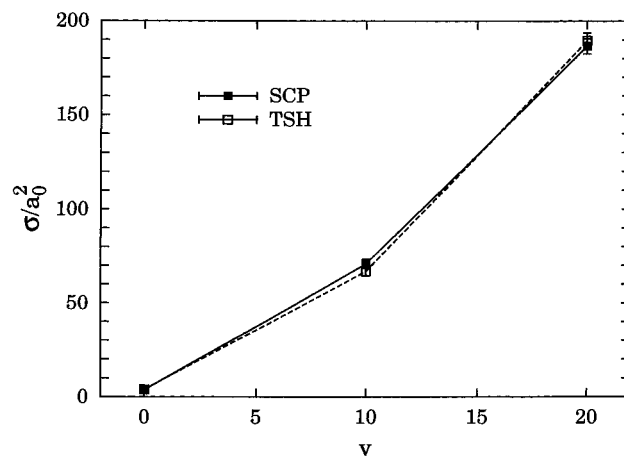


**Figure 9.** Dissociative cross sections as a function of the reactant Li<sub>2</sub> vibrational quantum number. The open squares are the TSH results, while the full squares represent the SCP ones.

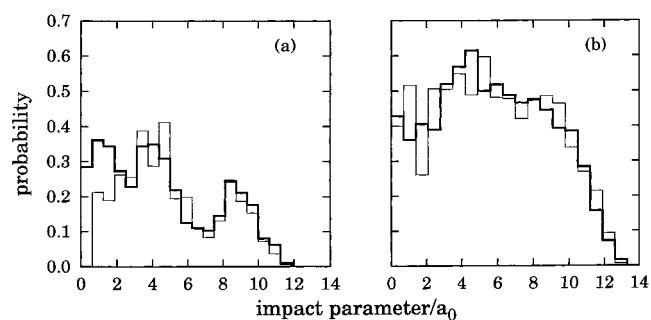


**Figure 10.** Opacity function for SCP (thick line) and TSH (thin line) methods at  $E_{tr} = 25 \text{ kcal mol}^{-1}$ : (a)  $\nu = 10$ ; (b)  $\nu = 20$ .

and perpendicular attacks. Inspection of Figures 2b and 3a suggests that such maxima are due to head-on collisions occurring at small (large) impact parameters for parallel (perpendicular) attacks. The potential wells are in turn expected to be responsible for the maximum at large (small) values of  $b$  for parallel (perpendicular) Li–Li<sub>2</sub> approaches. Figure 8c,d also shows that head-on collisions contribute more to dissociation in both methods. Because  $V_{11}$  is more attractive than  $V_{\perp}$ , the number of dissociative trajectories “captured” by the well is then expected to be bigger in SCP than TSH, as corroborated from Figure 8c,d. In fact, Table 3 shows that  $\sigma_{\parallel}$  and  $\sigma_{\perp}$  are both larger in SCP. Thus, it is reasonable to attribute the disagreement between the SCP and TSH values of  $\sigma_d$  with increasing  $E_{tr}$  to differences in the attractive parts of  $V_{11}$  and  $V_{\perp}$ .

Figure 9 shows  $\sigma_d$  as a function of  $\nu$ ; see also Table 1 and Table 2. We observe that  $\sigma_d$  and  $b_{\max}$  increase with  $\nu$  for both TSH and SCP, overlapping within their error bars. As the vibrational quantum number increases from  $\nu = 0$  to  $\nu = 10$  and  $\nu = 20$ , the energy necessary to break the Li–Li bond is seen to be significantly reduced (Figure 4). Thus, for  $\nu = 10$  and  $\nu = 20$ , a collision energy of  $25 \text{ kcal mol}^{-1}$  is enough to establish dissociation as the most probable event; see also section 3.2. Figures 7a and 10 also show that the reactive probability increases with  $\nu$  for most impact parameters. Similar patterns of the opacity functions are observed for both SCP and TSH results.

Figure 11 shows the opacity functions associated with parallel and perpendicular Li–Li<sub>2</sub> collisions; the dissociative cross sections are in Table 3. Clearly, both TSH and SCP results show similar trends for parallel and perpendicular attacks. For the former, the opacity function peaks at  $b = 0a_0$ , decreasing for

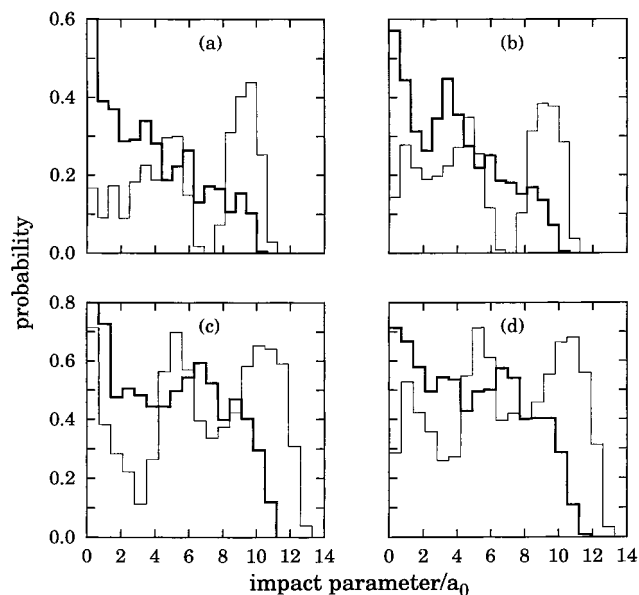


**Figure 11.** Opacity function for parallel (thick line) and perpendicular (thin line) Li–Li<sub>2</sub> attacks for  $\nu = 10$  (panels a and b) and  $\nu = 20$  (panels c and d) using both TSH (panels a and c) and SCP (panels b and d) methods. In all cases,  $E_{tr} = 25 \text{ kcal mol}^{-1}$ .

larger values of the impact parameter. This feature is more evident for  $\nu = 10$  (panels a and b) indicating that head-on collisions are most important to obtain dissociation; for  $\nu = 20$  (panels c and d), the parallel opacity function becomes broader as the vibrational energy gets closer to the dissociation threshold. Figure 11 also shows that the perpendicular opacity function has three maxima, two of which are attributable to a split of the “head-on maximum” (discussed above for  $E_{tr} = 80 \text{ kcal mol}^{-1}$ ) due to a larger amplitude of the vibrational motion; this is particularly clear for  $\nu = 20$  (panels c and d). The maximum at  $b \approx 0a_0$  seems less important for the dissociative process, especially for  $\nu = 10$ . Both facts stress the importance of head-on collisions for dissociation at  $E_{tr} = 25 \text{ kcal mol}^{-1}$  and hence explain the similar values of  $\sigma_d$  obtained in SCP and TSH methods.

#### 4. Conclusions

We have carried out trajectory studies of collision-induced dissociation for the Li + Li<sub>2</sub> system using the SCP and TSH semiclassical methods on realistic two-valued potential energy surfaces. The results show that both methods yield almost similar energy dependences for dissociative cross sections at translational energies close to the dissociation threshold; at higher values of  $E_{tr}$ , the SCP cross sections supersede TSH ones. The role of nonadiabatic effects and vibrational excitation of reagents have been also investigated. We have shown that the dissociation process is essentially governed by the particular features of  $V_-$  and  $V_{11}$  in the cases of TSH and SCP. Then, the discrepancies appear to be mainly due to the fact that the two methods used different representations: adiabatic for TSH versus diabatic for SCP. Because dissociative events have been associated essentially with head-on collisions, which are approximately dominated by similar repulsive forces in TSH and SCP approaches, we believe that such collisions are possibly responsible for the similarity of the results arising from these methods. In general, given the simplicity of TSH method and the fact that the SCP method may lead to “nonpure” molecular states, we are tempted to conclude that in its original form or in more sophisticated formulations<sup>35</sup> (not investigated in the

present work), such an approach has still a wide scope because exact quantum calculations cannot be done for most nonadiabatic studies of practical interest.

**Acknowledgment.** This work has been supported by Fundação para a Ciência e Tecnologia, Portugal, under programs PRAXIS and SAPIENS.

#### References and Notes

- (1) Tully, J. C.; Preston, R. K. *J. Chem. Phys.* **1971**, *55*, 562.
- (2) Blais, N. C.; Truhlar, D. G. *J. Chem. Phys.* **1983**, *79*, 1334.
- (3) Blais, N. C.; Truhlar, D. G.; Mead, C. A. *J. Chem. Phys.* **1988**, *89*, 6204.
- (4) Tully, J. C. *J. Chem. Phys.* **1990**, *93*, 1061.
- (5) Kuntz, P. J. *J. Chem. Phys.* **1991**, *95*, 141.
- (6) Chapman, S. *Adv. Chem. Phys.* **1992**, *82*, 423.
- (7) London, F. Z. *Electrochem.* **1929**, *35*, 552.
- (8) Eyring, H.; Polanyi, M. Z. *Phys. Chem. Abt.* **1931**, *12*, 279.
- (9) Sato, S. *J. Chem. Phys.* **1955**, *23*, 2465.
- (10) Varandas, A. J. C. *Int. J. Quantum Chem.* **1987**, *32*, 563.
- (11) Meyer, H. D.; Miller, W. H. *J. Chem. Phys.* **1979**, *70*, 3214.
- (12) Micha, D. A. *J. Chem. Phys.* **1983**, *78*, 7138.
- (13) Durup, J. *Chem. Phys. Lett.* **1990**, *537*, 173.
- (14) García-Vela, A.; Gerber, R. B.; Imre, D. G. *J. Chem. Phys.* **1992**, *97*, 7242.
- (15) Gerber, R. B.; Buch, V.; Ratner, M. A. *J. Chem. Phys.* **1982**, *77*, 3022.
- (16) Buch, V.; Gerber, R. B.; Ratner, M. A. *Chem. Phys. Lett.* **1983**, *101*, 44.
- (17) Alimi, R.; Gerber, R. B.; Hammerich, A. D.; Kosloff, R.; Ratner, M. A. *J. Chem. Phys.* **1990**, *93*, 6484.
- (18) Amarouche, M.; Gadea, F. X.; Durup, J. *Chem. Phys.* **1989**, *130*, 145.
- (19) Voronin, A. I.; Marques, J. M. C.; Varandas, A. J. C. *J. Phys. Chem. A* **1998**, *102*, 6057.
- (20) Topaler, M. S.; Hack, M. D.; Allison, T. C.; Liu, Y.-P.; Mielke, S. L.; Schwenke, D. W.; Truhlar, D. G. *J. Chem. Phys.* **1997**, *106*, 8699.
- (21) Topaler, M. S.; Truhlar, D. G. *J. Chem. Phys.* **1997**, *107*, 392.
- (22) Topaler, M. S.; Allison, T. C.; Schwenke, D. W.; Truhlar, D. G. *J. Phys. Chem.* **1998**, *102*, 1666.
- (23) Topaler, M. S.; Allison, T. C.; Schwenke, D. W.; Truhlar, D. G. *J. Chem. Phys.* **1998**, *109*, 3321.
- (24) Topaler, M. S.; Allison, T. C.; Schwenke, D. W.; Truhlar, D. G. *J. Chem. Phys.* **1999**, *110*, 687.
- (25) Marques, J. M. C.; Voronin, A. I.; Varandas, A. J. C. *Phys. Chem. Chem. Phys.* **1999**, *1*, 2657.
- (26) Volobuev, Y. L.; Hack, M. D.; Topaler, M. S.; Truhlar, D. G. *J. Chem. Phys.* **2000**, *112*, 9716.
- (27) Varandas, A. J. C. In *Reaction and Molecular Dynamics*; Laganá, A., Riganelli, A., Eds.; Lecture Notes in Chemistry, Vol. 75; Springer: Berlin, 2000; p 33.
- (28) Varandas, A. J. C.; Pais, A. A. C. C. *J. Chem. Soc., Faraday Trans.* **1993**, *89*, 1511.
- (29) Pais, A. A. C. C.; Nalewajski, R. F.; Varandas, A. J. C. *J. Chem. Soc., Faraday Trans.* **1994**, *90*, 1381.
- (30) Parlant, G.; Gislason, E. A. *J. Chem. Phys.* **1989**, *91*, 4416.
- (31) Tully, J. C. *Int. J. Quantum Chem., Quantum Chem. Symp.* **1991**, *25*, 299.
- (32) Hammes-Schiffer, S.; Tully, J. C. *J. Chem. Phys.* **1994**, *101*, 4657.
- (33) Muller, U.; Stock, G. *J. Chem. Phys.* **1997**, *107*, 6230.
- (34) Volobuev, Y. L.; Hack, M. D.; Truhlar, D. G. *J. Phys. Chem.* **1999**, *103*, 6225.
- (35) Zhu, C.; Teranishi, Y.; Nakamura, H. *Adv. Chem. Phys.* **2001**, *117*, 127.
- (36) Zhu, C.; Kamisaka, H.; Nakamura, H. *J. Chem. Phys.* **2001**, *115*, 11036.
- (37) Osherov, V. I.; Ushakov, V. G. *Sov. Phys. Dokl.* **1977**, *22*, 499.
- (38) Dehareng, D.; Chapuisat, X.; Lorquet, J. C.; Galloy, C.; Raseev, G. *J. Chem. Phys.* **1983**, *78*, 1246.
- (39) Desouter-Lecomte, M.; Dehareng, D.; Leyh-Nihant, B.; Praet, M. T.; Lorquet, A. J.; Lorquet, J. C. *J. Phys. Chem.* **1985**, *89*, 214.
- (40) Last, I.; Baer, M. *J. Chem. Phys.* **1985**, *82*, 4954.
- (41) Takayanagi, T.; Kurosaki, Y.; Ichihara, A. *J. Chem. Phys.* **2000**, *112*, 2615.
- (42) Varandas, A. J. C. *Adv. Chem. Phys.* **1988**, *74*, 255.
- (43) Varandas, A. J. C. *Chem. Phys. Lett.* **1992**, *194*, 333.